THE JOURNAL OF PHYSICAL CHEMISTRY B

Article

pubs.acs.org/JPCB

Time-Resolved Spectroscopic Study of the Photochemistry of Tiaprofenic Acid in a Neutral Phosphate Buffered Aqueous Solution from Femtoseconds to Final Products

Tao Su, Jiani Ma, Ming-De Li, Xiangguo Guan, Lihong Yu, and David Lee Phillips*

Department of Chemistry, The University of Hong Kong, Pokfulam Road, Hong Kong, P.R. China

Supporting Information

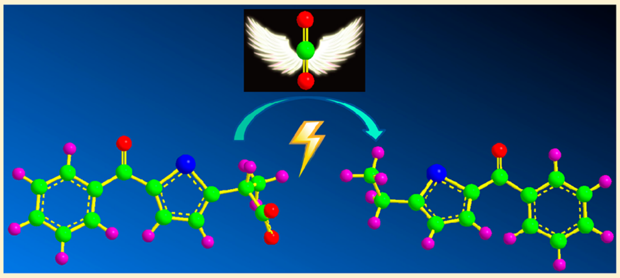

ABSTRACT: The photo-decarboxylation and overall reaction mechanism of tiaprofenic acid (TPA) was investigated by femtosecond transient absorption (fs-TA), nanosecond transient absorption (ns-TA), and nanosecond time-resolved resonance Raman (ns-TR^3) spectroscopic experiments in a neutral phosphate buffered solution (PBS). In addition, density functional theory (DFT) calculations were presented to help interpret the experimental results. Resonance Raman and DFT calculation results revealed that the deprotonated tiaprofenic acid (TPA$^-$) form was the primary species that is photoexcited in a near neutral PBS aqueous solution. The fs-TA experimental data indicated that the lowest lying excited singlet state S_1 underwent an efficient intersystem crossing process (ISC) to quickly transform into the lowest lying excited triplet state T_1 that then undergoes decarboxylation to generate a triplet biradical species (TB^3). ns-TA and ns-TR^3 results observed a protonation process for TB^3 to produce a neutral species (TBP^3) that then decayed via ISC to produce a singlet TBP species that further reacted to make the final product (DTPA). A comparison of the present results for TPA$^-$ with similar results for the deprotonated form of ketoprofen (KP$^-$) in the literature was done to investigate how the thiophene moiety in TPA$^-$ that replaces one phenyl ring in KP$^-$ affects the reaction mechanism and photochemistry of these nonsteroidal anti-inflammatory drugs (NSAIDs).

INTRODUCTION

Nonsteroidal anti-inflammatory drugs (NSAIDs) are widely utilized for the treatment of inflammation and inflammatory diseases even though these types of drugs may cause various adverse side effects such as cutaneous phototoxic responses in some patients.[1,2] Tiaprofenic acid, 2-(5-[2-benzoyl] thienyl) propionic acid (TPA), is a typical NSAID drug that can act as a photosensitizer against cell components.[3,4] TPA is usually dispensed and used as a racemic mixture for the treatment of acute and chronic arthritis and osteoarthritis.[5] Several investigations have been reported for the photochemistry of TPA and some analogues.[6−17] One series of studies proposed that the photo-decarboxylation for TPA$^-$ involved the (n, π*) triplet state of TPA$^-$ as a key intermediate and the decarboxylation occurred in a manner similar to those observed for some other NSAIDs that contain a benzophenone (BP) group.[2,18−21] The triplet (n, π*) was proposed to have a higher energy and to exist in thermal equilibrium with the lowest lying triplet (π, π*) state. Upon absorption of a photon, TPA reaches an excited singlet state and quickly undergoes an intersystem crossing (ISC) process to the lowest lying excited triplet (π, π*) state (denoted as TPA^3-1) with an approximately 90% efficiency. The transformation to an upper excited triplet (n, π*) state (TPA^3-2) by thermal activation of an about 7−10 kJ/mol energy barrier was proposed to lead to a decarboxylation reaction that has an about 25% efficiency[13,22,23] to form a triplet biradical species (TB^3) which subsequently undergoes ISC to produce the singlet form (TB). TB^3 and TB are both in equilibrium with their conjugate acids. Subsequent protonation of TB leads to the formation of the major photoproduct, 2-benzoyl-5-ethylthiophene (DTPA), in aqueous solutions (see Scheme 1 for an overview of the proposed mechanism).[3]

The photo-decarboxylation of TPA was also investigated by density functional theory (DFT) calculations, and another mechanism involving excitation and photo-decarboxylation of the deprotonated form was proposed.[24] This work concluded that TPA is not capable of undergoing the photo-decarboxylation reaction from any of the lowest lying excited singlet states, since the energy curves for those processes are all endothermic or are associated with very high barriers. However, once the system has undergone efficient ISC to a corresponding triplet state, the photo-decarboxylation reaction can occur spontaneously. The decarboxylated product of TPA has several options for further reaction that can lead to the formation of the closed-shell ethyl derivative, alcohol or ketone species, or a peroxyl radical capable of initiating lipid peroxidation reactions. In several of these reactions, either superoxide anions or singlet oxygen can be formed. It was concluded that the most likely pathway involves the protonation of the terminal (decarboxylated) carbon, followed by decay from the triplet to the corresponding singlet ground

Received: October 18, 2012
Published: December 11, 2012

dx.doi.org/10.1021/jp310315f | J. Phys. Chem. B 2013, 117, 811−824

Scheme 1. Proposed Photo-Decarboxylation Reaction Pathway of TPA in PBS Solution by Some Previous Experimental Studies

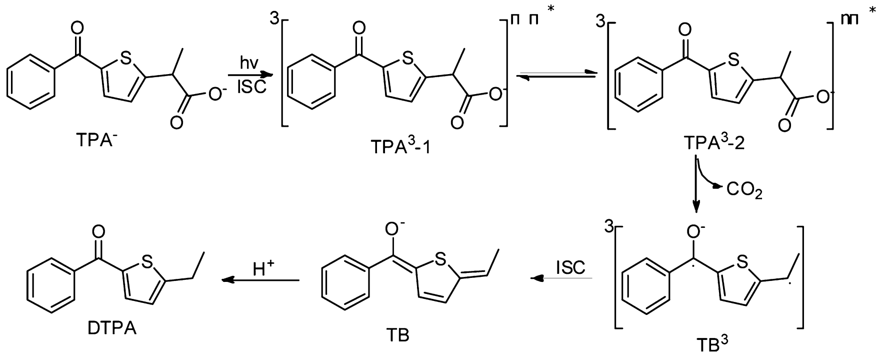

Scheme 2. Proposed Photo-Decarboxylation Reaction Pathways of TPA from Previous DFT Computational Results[24]

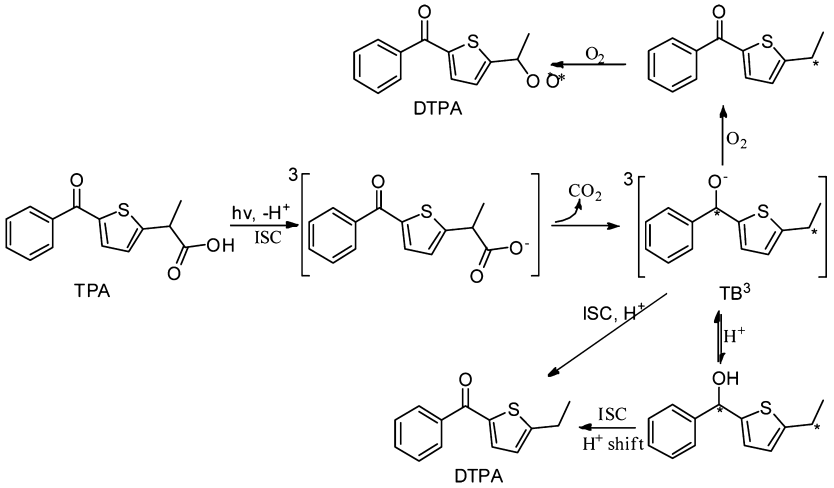

state. Protonation of the ketone connecting the two rings is also possible, but this leads to the generation of a compound with a long lifetime that requires a proton shift for further decay (see Scheme 2 for a summary of the proposed mechanisms).

In the studies done so far for TPA, only a few experimental techniques were used to investigate the transient species during the course of the photo-decarboxylation reaction of TPA in aqueous solutions. Laser flash photolysis (LFP) played an important role for the initial assignment of the transient species involved in the photo-decarboxylation process of TPA. However, it is sometimes difficult to clearly distinguish various transient species that have similar electronic absorption spectra and time scales in transient absorption experiments.[20,22] In these cases, it is sometimes useful to employ time-resolved vibrational spectroscopy techniques that can more clearly distinguish the various transient species present by their vibrational frequencies that contain structural information and can serve as a fingerprint for each species. Recently, we have utilized ns-TR^3 spectroscopy to carry out a number of studies on the photochemistry of BP and NSAID drugs like ketoprofen (KP) that contain a benzophenone group. These studies provided new insight into the identities, structures, and properties of several transient species associated with photochemical reactions observed in these benzophenone containing molecular systems.[25−32] While both TPA and BP containing NSAID drugs like KP both contain an aromatic carbonyl moiety, the carboxyl containing side chain is attached to a different ring group in these two compounds, as shown in Figure 1. The carboxyl containing side chain is attached to a phenyl group in KP, while it is attached to a thiophene group in TPA. Here, we have used femtosecond transient absorption spectroscopy (fs-TA), nanosecond transient absorption spectroscopy (ns-TA), and time-resolved resonance Raman (TR^3) spectroscopy to obtain valuable information about the identities, structures, and properties of the transient species from femtoseconds to the formation of the final product DPTA. In order to mimic the physiological environment, the predominantly PBS mixed solvent of 70% PBS/30% acetonitrile (by volume ratio) was used due to the low solubility of TPA in PBS. The results obtained for TPA here are compared and contrasted with the photo-decarboxylation reactions of KP so as to learn more about how the use of a thiophene versus a phenyl ring connecting the carbonyl group to the carboxyl containing side chain affects the photophysical and photochemical processes in these NSAID drugs.

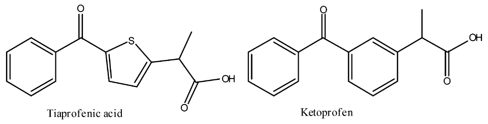

Figure 1. The chemical structures of TPA and KP.

■ EXPERIMENTAL AND COMPUTATIONAL METHODS

Materials. TPA was commercially obtained from Tractus (with >96% purity) and used as received. Unless noted otherwise, all of the sample solutions of TPA were used in a mixture of PBS and MeCN with a volume ratio of 7:3. The solutions used in the resonance Raman and ns-TR^3 experiments had a concentration of 1.0 mM. The pH 7.4 phosphate buffer solution was prepared using 29.38 g of $Na_2HPO_4{\cdot}12H_2O$ and 2.48 g of KH_2PO_4/L to give a 0.1 M solution.

Steady-State UV/vis Absorption. Steady-state absorption spectra were recorded on a PerkinElmer Lambda 19 UV/vis spectrometer using a 1 cm path length quartz cuvette.

fs-TA Experiments. The fs-TA measurements were performed on the basis of a femtosecond Ti:sapphire regenerative amplified Ti:sapphire laser system and an automated data acquisition system. The amplifier was seeded with the 120 fs output from the oscillator. The probe pulse was obtained by using approximately 5% of the amplified 800 nm output from the amplifier to generate a white-light continuum (320−800 nm) through a CaF_2 crystal. The maximum extent of the temporal delay was about 3300 ps for the optical stage used in the experiments, and the instrument response function was determined to be about 150 fs. At each temporal delay, the data were averaged for 2 s. The probe beam was split into two before passing through the sample with one beam traveling through the sample and the other one passing directly through the reference spectrometer that monitors the fluctuations in the probe beam intensity. Fiber optics were coupled to a multichannel spectrometer with a CMOS sensor that had a 1.5 nm intrinsic resolution. For the present experiments, the sample solutions were excited by a 267 nm pump beam (the third harmonic of the fundamental 800 nm light from the regenerative amplifier). Sample solutions of 60 mL were employed in a flowing 2 mm path-length cuvette with a sample UV/vis intensity of about 1 throughout the data acquisition. The data were stored as three-dimensional (3D) wavelength−time−absorbance matrices that were exported for use with the fitting software.

ns-TA Experiments. Nanosecond time-resolved transient absorption (ns-TA) measurements were carried out with a LP920 laser flash spectrometer provided by Edinburgh Instruments Ltd. The probe light source was a 450 W ozone free Xe arc lamp with 10 Hz to single shot operation in a sample chamber with an integral controller, high speed pump and probe port shutters, sample holder, and filter holders. The lamp produces a continuous spectrum between 150 and 2600 nm. Measurements of the ns-TA spectra were performed according to the following procedure. Fresh sample solutions were excited by a Q-switched Nd:YAG laser (fourth harmonic line at $\lambda = 266$ nm). The probe light from a pulsed xenon arc lamp passed through various optical elements, samples, and a monochromator before being detected by a fast photomultiplier tube and recorded with a TDS 3012C digital signal analyzer. In the kinetics mode, a photomultiplier detector or InGaAs PIN detector was used and the transient signal was acquired using a fast, high resolution oscilloscope. In the spectral mode, an array detector was fitted to the spectrograph exit port to measure a full range of wavelengths simultaneously. About 4 mL solutions were employed in a 10 mm path-length cuvette with a sample of UV/vis intensity of about 1 throughout the data acquisition.

ns-TR^3 Experiments. The ns-TR^3 experiments were done using an experimental apparatus and methods discussed in detail previously,[33,34] so only a brief description will be given here. The 266 nm pump laser pulse and a 341.5 nm probe laser pulse (generated from the second Stokes hydrogen Raman shift laser line from the fourth harmonic) were used to detect transient species and the final product arising from photodecarboxylation. The energy for the pump and probe pulses was in the range 2.5−3.5 mJ with a 10 Hz repetition rate. The two Nd:YAG lasers were synchronized electronically by a pulse delay generator to control the time delay of the pump and probe lasers with the time delay between the laser pulses monitored by a fast photodiode and 500 MHz oscilloscope, and the time resolution for the ns-TR^3 experiments was approximately 10 ns. The pump and probe laser beams were lightly focused onto the flowing sampling system, and the Raman light was collected using reflective optics into a spectrometer whose grating dispersed the light onto a liquid nitrogen cooled CCD detector. The Raman signal was accumulated for 30 s by the CCD before reading out to an interfaced PC computer, and 10−20 scans of the signal were added together to get a resonance Raman spectrum. The ns-TR^3 spectra presented here were obtained by the subtraction of a resonance Raman spectrum with a negative time delay of −100 ns (probe-before-pump spectrum) from the resonance Raman spectrum with a positive time delay (pump−probe spectrum), and the Raman shifts were calibrated by the known MeCN solvent Raman bands with an estimated accuracy of 5 cm^{-1}.

Density Functional Theory (DFT) Computations. DFT calculations were done employing the Becke three-parameter hybrid method with the Lee−Yang−Parr correlation functional approximation (U)B3LYP method with a 6-311G(d,p) basis set. The Raman spectra were obtained using a determination of the Raman intensities from transition polarizabilities calculated by numerical differentiation, with an assumed zero excitation frequency. A Lorentzian function with a 15 cm^{-1} bandwidth for the vibrational frequencies and an individual frequency scaling factor (see Table2) was used in the comparison of the calculated results with the experimental spectra. No imaginary frequency modes were observed at the stationary states of the optimized structures, and only one imaginary frequency was observed for the saddle point transition state structures. The isomerization process was explored by optimizing the structures of the reactant, transition states, and product complexes. Transition states were located using the Berny algorithm. Frequency calculations at the same level of theory were performed to confirm that the structures were at local minima with all-real frequencies or at transition states with only one imaginary frequency. The nature of the transition states was determined by analyzing the motion by the eigenvector associated with the imaginary frequency. Intrinsic reaction

Table 1. Absorption Band(s) and Assignments of the Transient Species Observed in the fs-TA Spectra (See Text for Details)

transient species	absorption peaks (nm)
1, S_n	340
2, S_1	360
3, T_1	360, 600
4, TB^3	360, 420, 600

Table 2. The Different Scaling Factors Used for the Normal Raman Spectra to Compare to the Individual Transient Species ns-TR^3 Spectra

transient species	TPA^-	TB^3	TBP^3	TBP	DTPA
scaling factors	0.961	0.983	0.99	0.974	0.969

coordinates (IRC)[35−37] were calculated for the transition states to confirm the relevant structures connect the two relevant minima. The polarizable continuum model (PCM) is used for evaluating the (bulk) solvent effects.[38] No imaginary frequency modes were observed at the stationary states of the optimized structures. All the calculations were done using the Gaussian 03 program[39] installed on the High Performance Computing cluster at the Computer Centre in The University of Hong Kong.

■ RESULTS AND DISCUSSION

UV/vis Absorption and Resonance Raman Spectra for TPA in Neutral Aqueous PBS Solution. The UV/vis experiments were conducted in both pure acetonitrile (MeCN) and neutral PBS aqueous solutions, as shown in Figure 2. The absorption spectrum of TPA (in its dissociated form) in the neutral PBS aqueous solution is characterized by intense bands with maxima at 314 and 261 nm and a weak tail extending up to 380 nm. The solvent polarity affects the spectrum to a slight extent so that the two main bands at 314 and 261 nm shift to 300 and 259 nm, respectively, in pure MeCN which has a lower solvent polarity. In contrast, the absorption at $\lambda > 360$ nm does not experience any significant solvent shift.

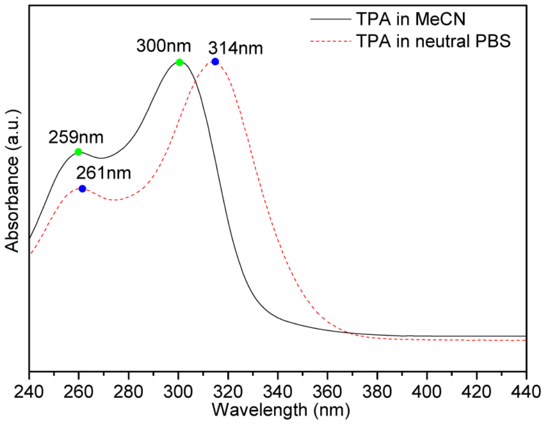

Figure 2. UV/vis absorption spectra of TPA in pure MeCN and neutral aqueous PBS solvents.

TD-DFT calculations were done to simulate the absorption spectrum (see Figure 1S and Table 2S in the Supporting Information). Frontier orbitals were also calculated at the B3LYP/6-311G(d,p) level of theory and indicate that both of the two main bands are characteristic of (π, π^*) absorption transitions. The band at 314 nm is mainly due to the transition from HOMO-3 to LUMO, and the band at 261 nm is mainly associated with the transition from HOMO-3 to LUMO+2 (see Figure 2S, Supporting Information). It is known that the presence of an electron-donating group has little effect on the (π, π^*) band near 260 nm but induces a strong absorption at longer wavelengths.[10] The 267 nm third harmonic of the fundamental 800 nm light from the regenerative amplifier was used as the pump laser pulse in the fs-TA experiments reported here. The 266 nm fourth harmonic of the fundamental 1064 nm light from a Nd:YAG laser was employed for the pump laser pulse in the ns-TA and ns-TR^3 experiments reported here. For all of the time-resolved experiments reported here, the pump laser pulses excite the (π, π^*) band near 260 nm.

Previous studies found that the photo-decarboxylation reaction takes place from the deprotonated form of TPA in a PBS aqueous solution;[20,22] however, no explicit structural characterization of the properties of the ground electronic state of the substrate species being excited were presented. In this work, resonance Raman experiments were performed in a basic aqueous solution at pH 13 and a neutral PBS aqueous solution. Since the pK_a of TPA is reported[40] to be 3.0, the deprotonated form of TPA (denoted as TPA$^-$) is expected to be the main species present in a pH 13 aqueous solution. The resonance Raman spectrum obtained in a pH 13 aqueous solution is compared with the predicted normal Raman spectrum computed at the B3LYP/6-311G(d,p) level of theory in Figure 3. Inspection of Figure 3 shows there is good agreement between the experimental resonance Raman spectrum with the predicted normal Raman spectrum, and this indicates that the TPA$^-$ species is the main form present in the pH 13 aqueous solution. Most of the resonance Raman bands observed for the TPA$^-$ species are due to vibrations associated with the ring C═C stretching, C—C stretching, and C═O stretching motions located in the 800−1800 cm^{-1} region. For instance, the C═C stretching and C═O stretching modes are attributed to the Raman bands at 1637 and 1663 cm^{-1}. The ring breathing vibrational modes are associated with the Raman bands at 1016 and 1156 cm^{-1}. More detailed information about the comparison of the experimental and calculated Raman spectra and the assignments of the vibrational motions is listed in Table 7S of the Supporting Information.

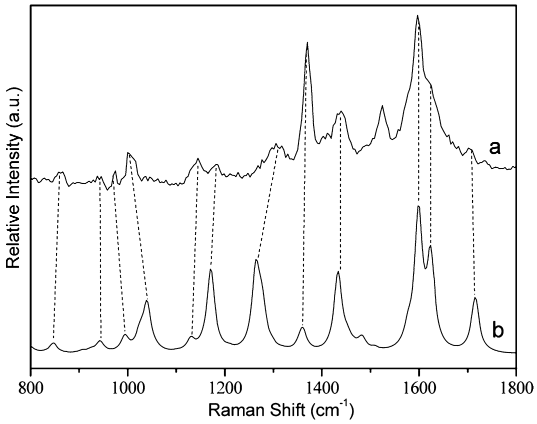

Figure 3. Comparison of (a) the experimental resonance Raman spectrum of TPA obtained in a basic aqueous solution with pH 13 with (b) the calculated ground state normal Raman spectrum of TPA$^-$.

The resonance Raman spectrum for TPA in a neutral PBS aqueous solution was also obtained and compared with the resonance Raman spectrum acquired in the pH 13 aqueous solution, as shown in Figure 4. Examination of Figure 4 reveals that the spectra are nearly identical, which indicates that the species in the neutral PBS aqueous solution is also the TPA$^-$ form of the molecule.

The optimized structures of the TPA and TPA$^-$ ground states are presented in Figure 5 (top) and (middle). Inspection of Figure 5 reveals that there is a significant difference in the $C_{21}-C_{27}$ bond length for TPA and TPA$^-$, 1.526 and 1.627 Å, respectively. The $C_{21}-C_{27}$ bond length for TPA$^-$ is longer than that of TPA and appears to be close to that of a normal single carbon−carbon bong length. This indicates the bond energy of the $C_{21}-C_{27}$ bond for the TPA$^-$ form of the molecule may be

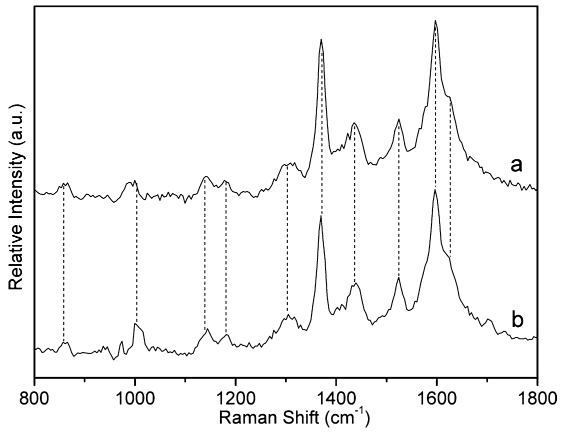

Figure 4. Shown is a comparison of (a) the resonance Raman spectrum of TPA obtained in a neutral PBS aqueous solution with (b) the resonance Raman spectrum of TPA obtained in a basic aqueous solution at pH 13.

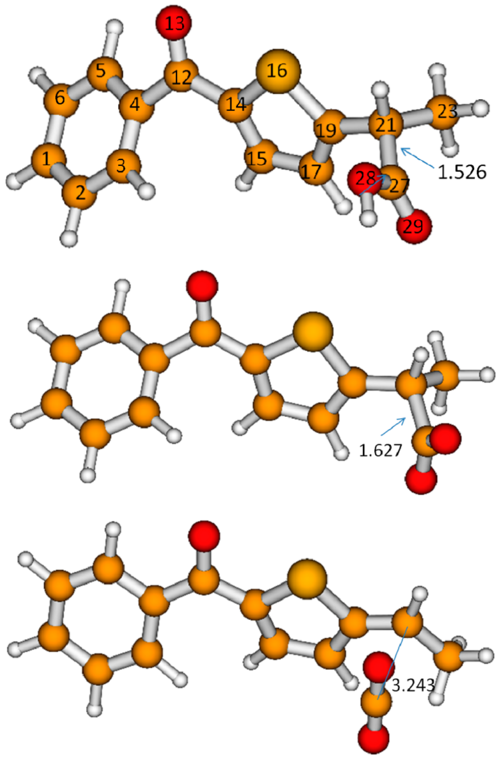

Figure 5. Shown are the optimized geometry structures calculated at the (U)B3LYP/6-311G(d,p) level of theory for the ground singlet state of TPA (top), the ground state of TPA$^-$ (middle), and the triplet state TPA$^-$ species (bottom).

significantly weaker and easier to cleave than for the TPA neutral form of the molecule. When we attempted to optimize the structure of the triplet state TPA$^-$ species, we found that the cleavage of the bond located at $C_{21}-C_{27}$ took place spontaneously (see Figure 5, bottom structure), whereas this behavior was not observed for triplet state TPA species. These results are consistent with those reported by Eriksson and co-workers.[24]

fs-TA and ns-TA Spectroscopy Investigations on TPA$^-$. Figure 6 displays the fs-TA spectra obtained after 267 nm excitation of TPA in a neutral PBS aqueous solution from 0 to 3000 ps. To clearly indicate the spectral changes occurring on different time scales, the spectra of the early (0.2−1, 1−11 ps) and later (after 11 ps) delay times are given separately. At the beginning, a weak band assigned to intermediate **1** at about 340 nm grew in rapidly and red-shifted to 360 nm. This indicates intermediate **1** decays to generate another intermediate **2** within a very short time (see Figure 6a). Subsequently, the absorption band at 360 nm begins to decrease gradually and is accompanied by the generation of a new absorption band at about 600 nm that is assigned to intermediate **3** up to 11 ps. When the band at 600 nm reaches a maximum, the band at 360 nm still does not completely decay and this indicates that intermediate **3** also has some absorption at about 360 nm. An isosbestic point was observed at around 420 nm between the bands at 360 and 600 nm, and this suggests that intermediate **2** is the precursor for intermediate **3**. With the evolution of the time delay, intermediate **4** associated with the absorption band around 415 nm was formed. The growth of the absorption band at 415 nm supplies evidence for the formation of intermediate **4**, and two new isosbestic points located at about 380 and 440 nm indicate that intermediate **4** was generated from the decay of intermediate **3**.

The first change observed at very early times (before 1 ps) is assigned to the internal conversion (IC) process from intermediate **1** (assigned to the higher excited singlet S_n state species) to intermediate **2** (assigned to the lowest lying exicted singlet state S_1). This assignment is consistent with the typical IC photophysical process on a femtosecond time scale.[41] Due to the high efficiency of the intersystem crossing (ISC) for TPA which can be up to 0.9,[20] the subsequent process in the spectral development in the fs-TA spectra can be reasonably attributed to ISC from the S_1 state to intermediate **3** that is assigned to the lowest lying excited triplet state T_1. As mentioned before, carbon dioxide will leave spontaneously when we attempt to optimize the triplet state TPA$^-$ species in some DFT calculations, which is consistent with previously reported DFT results of Eriksson and co-workers[24] and also similar to analogous computational results for KP.[43] Therefore, we think the triplet state T_1 of TPA$^-$ (e.g., intermediate **3**) spontaneously decaboxylates to produce intermediate **4**. DFT calculations were performed to optimize the structure of intermediate **4**, and the results for its charge and spin distribution are displayed in Figure 7. Examination of Figure 7 (left) reveals that much of the negative charge is located on the O_7 atom with some modest negative charge also located on the C_3, C_1, and C_8 atoms (see Figure 3S in the Supporting Information for the labeling of the atoms). The positive charge was mainly situated on the C_6 atom with some positive charge also located on the S_2, C_{14}, and C_{15} atoms. Further inspection of Figure 7 (right) shows that around half of the spin density is located on the C_8 atom and most of the remaining spin is located on the C_3, C_6, and O_7 atoms (see Table 1S in the Supporting Information for details). On the basis of these results, it appears that intermediate **4** is a species that has biradical character and is denoted as TB^3 with a structure shown in Figure 3S (Supporting Information).

The assignment of TB^3 to intermediate **4** was further supported by a predicted absorption spectrum calculated at the BPW91/CC-PVDZ level of theory. The predicted absorption spectrum was depicted using Gausssum 2.2[44] with a fwhm of 7000 cm^{-1} and is shown in Figure 6d (see Table 3S, Supporting Information, for details of these computational results). Examination of Figure 6d shows that three strong absorption bands are clearly seen and are located at 350, 450, and 680 nm,

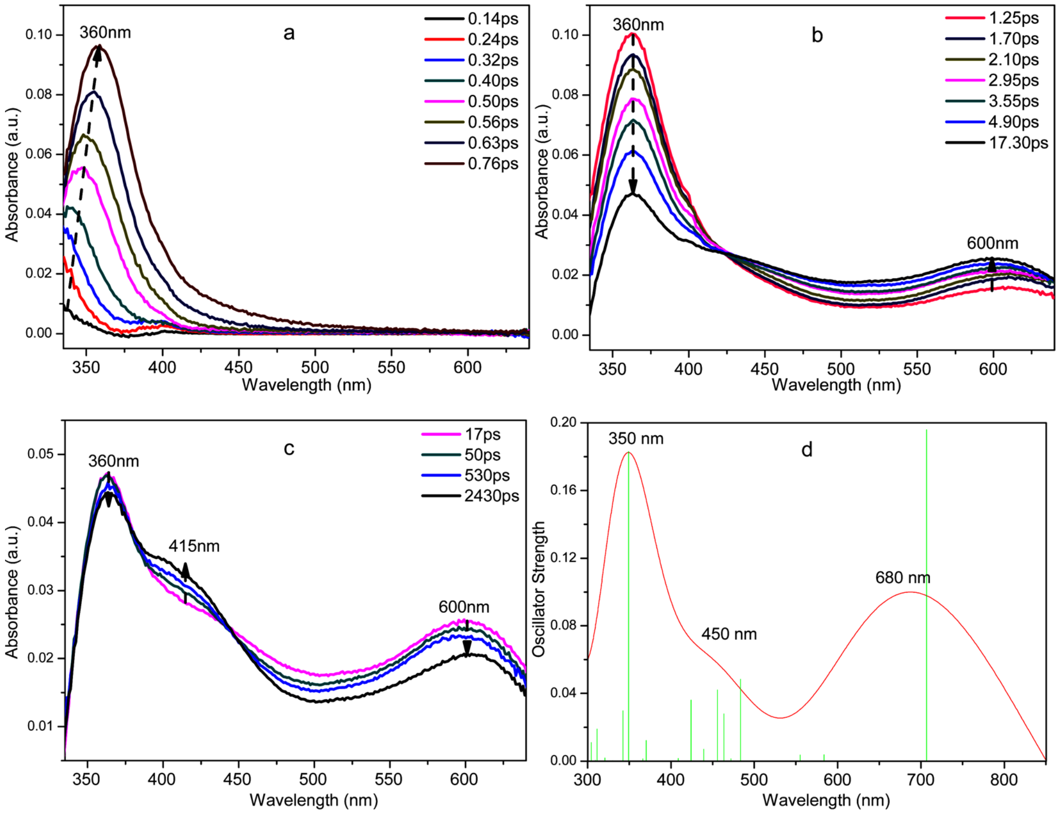

Figure 6. (a−c) The fs-TA spectra obtained for TPA in a neutral PBS aqueous solution and (d) the predicted absorption spectrum of the TB^3 intermediate from TD-DFT calculations done at the BPW91/CC-PVDZ level of theory (see text for details).

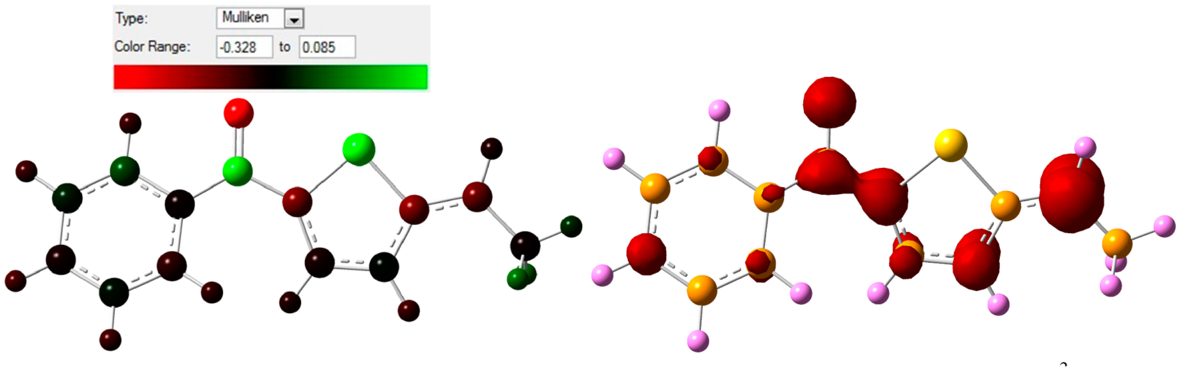
Type: Mulliken

Color Range: -0.328 to 0.085

Figure 7. Mulliken charge distribution (left) and spin distribution (right) for the TB^3 species calculated at the UB3LYP/6-311G(d,p) level of theory.

respectively. Taking into consideration that the current level of theory may have an error of about 0.2 eV, the TD-DFT predicted absorption spectrum can be regarded to be in comparatively good agreement with the experimental absorption spectrum.

Table 1 provides a summary of the transient species observed in the fs-TA spectra along with the tentative assignments of the intermediates and their approximate absorption band maxima observed in the experimental spectra.

To better understand the photophysical conversion processes seen at early times in the fs-TA spectra, the kinetics were monitored at 360 and 600 nm, respectively. The experimental results and a fitting of the data at 360 nm within 20 ps are shown in Figure 8a. Because both S_n and S_1 have contributions to the absorption band at 362 nm, a biexponential function was employed to fit the kinetics a best fit found time constants of $\tau_1 = 120 \pm 17$ fs and $\tau_2 = 2.7 \pm 0.06$ ps. The very short growth time (120 fs) is attributed to a fast IC process from S_n to S_1. Furthermore, as a result of the energies being close to each other for the lowest lying excited singlet state and the excited triplet, the ISC process is also easy to take place and we attribute the time constant of 2.7 ps to the ISC process to convert S_1 to T_1. To investigate the subsequent dynamical change taking place after the ISC process produces T_1, the kinetics of the aborption band at 600 nm was monitored, and its best-fit to the data is presented in Figure 8b. The growth and decay of the spectral data at 600 nm were well fit by a biexponential function with time constants of $\tau_1 = 3.0 \pm 0.24$ ps and $\tau_2 = 320 \pm 67$ ps. The shorter time constant of 3.0 ps was assigned to the formation time of T_1 and agrees well with the decay time constant of 2.7 ps for the S_1 state monitored at 360 nm. The T_1 state then appears to undergo a prompt decarboxylation reaction to form TB^3 with a time constant of 320 ps that was monitored at 600 nm. fs-TA experiments were

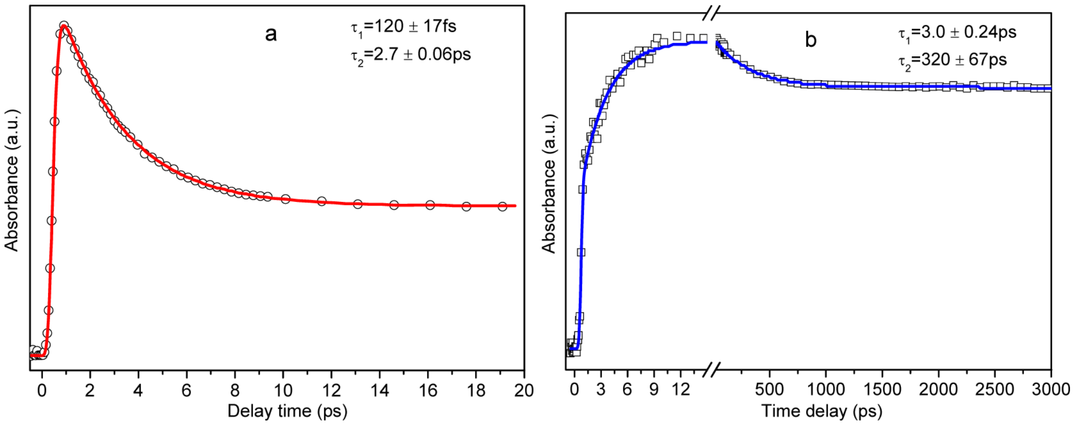

Figure 8. Kinetics and their fitting plots of the TPA fs-TA data in neutral PBS aqueous solution (a) at 360 nm within 20 ps and (b) at 600 nm within 3000 ps.

also done in pure MeCN for comparison purposes, and these spectra are displayed in Figure 4S (Supporting Information) along with the kinetics and relevant fitting plots of the absorption band at 350 nm. MeCN is an inert solvent with a lower polarity relative to pure water, so it can serve to stabilize a (n, π^*) triplet compared with a higher polarity water solvent. The time constants observed after 267 nm excitation of TPA in pure MeCN from a best-fit of a biexponential function to the data were $\tau_1 = 296 \pm 29$ fs and $\tau_2 = 2.4 \pm 0.17$ ps, respecitvely. The first time constant of $\tau_1 = 296$ fs can be attributed to IC from S_n to S_1, and the second time constant of $\tau_2 = 2.4$ ps can be atttributed to ISC from S_1 to T_1. These two time constants are practially identical with those obtained in a neutral PBS aqueous solution which suggests there is not much solvent polarity dependence for the IC from S_n to S_1 and the ISC from S_1 to T_1 for TPA. We note that many investigations on an analogous NSAID drug, KP,[42,45−47] indicate that photodecarboxylation prefers to proceed from the lowest lying triplet state and the data above suggests that the TPA decarboxylation reaction probably occurs in a similar manner.

The first and second excited triplet state (T_1 and T_2) geometries were optimized using the TD-DFT method, and the frontier orbitals obtained are shown in Figure 9. Analysis of the TD-DFT results indicates the HOMO and LUMO correspond to the T_1 transition and the T_2 transition is associated with the HOMO-1 to LUMO transition. Inspection of Figure 9 reveals that there is a (n, π^*) transition character for T_1 and a (π, π^*) transition character for T_2. This is consistent with the experimental results obtained from the fs-TA experiments done in both pure MeCN solvent and in a neutral PBS aqueous solution.

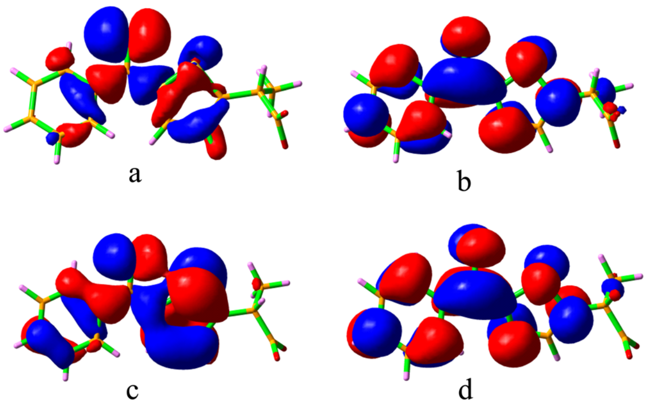

Figure 9. Shown are the DFT calculated frontier orbitals for the excited state triplet TPA^- involved in (a) the T_1 HOMO, (b) the T_1 LUMO; (c) the T_2 HOMO-1, and (d) the T_2 LUMO.

To investigate the photochemistry of TPA in neutral PBS aqueous solution on the nanosecond and microsecond time scales, ns-TA experiments were performed. Figure 10 presents ns-TA spectra obtained after 266 nm excitation of TPA in a neutral PBS aqueous solution under nitrogen-saturated conditions. The profile of the spectrum at 0 ns delay time is characterized by three absorption bands with maxima at about 360, 420, and 600 nm, and this absorption spectrum very closely resembles the 3000 ps spectrum observed in the fs-TA spectra. This implies the 0 ns spectrum in the ns-TA experiments and the 3000 ps spectrum in the fs-TA experiments are seeing the same transient species and have the same assignment. With time evolution, the absorption band at 360 nm increases along with a slight red shift to 369 nm, and this is accompanied by a substantial decline of intensity in the absorption band at 420 nm within 2 μs. Subsequently, the absorption band at 369 nm begins to decrease gradually with a marginal blue shift, and this is accompanied by a new absorption band increasing in intensity at about 450 nm within

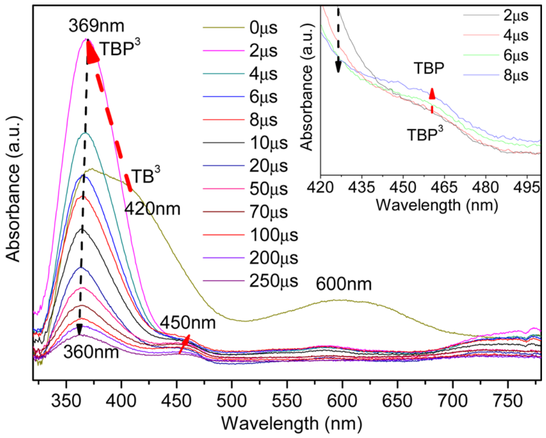

Figure 10. The ns-TA spectra obtained after 266 nm excitation of TPA in a neutral PBS aqueous solution under nitrogen-saturated conditions. Inset: An enlarged frame of spectra between 420 and 500 nm observed from 2 to 8 μs is also shown.

8 μs (see Figure 10, inset). Finally, both absorption bands at about 360 and 450 nm decreased progressively and the decay time for both occurred on the microsecond time scale. The absorption bands observed at 0 ns delay time can be assigned to the TB^3 due to the close similarity with the fs-TA spectrum observed at 3000 ps. The TB^3 species can undergo protonation to give a triplet neutral species that is denoted here as TBP^3. Since the pK_a of around 8.2[22] for TB^3 is higher than the pH value of about 7.4 in the neutral PBS aqueous solution examined here, the protonation of the TB^3 species to form the TBP^3 species appears to be a likely process to observe. DFT calculations were done for this protonation reaction and no transition state (TS) was found, indicating the protonation process proceeds spontaneously under relatively acidic conditions. After the protonation reaction to make the TBP^3 species, an ISC process can take place to produce the singlet TBP species which has absorption bands at about 360 and 450 nm. The results of DFT calculations for the free energies of the TBP^3 and TBP species found that TBP has a lower energy than TBP^3 (see the Supporting Information for details). The optimized structure of TBP is shown in Figure 11, and this structure exhibits an obvious enol character for the TBP intermediate. The predicted absorption spectrum of TBP^3 obtained from the TD-DFT calculations performed at the (U)B3LYP/6-311G(d,p) level of theory with consideration of the solvation effect by means of the PCM model using UAHF radii (Tables 4S and 5S, Supporting Information) is compared with the experimental spectrum in Figure 12. Inspection of Figure 12 reveals that the predicted TBP^3 absorption spectrum has one strong band located at 375 nm and one weak band located at 552 nm. Similarly, the predicted TBP absorption spectrum has a very strong absorption band at about 400 nm and a weak band located at about 320 nm.

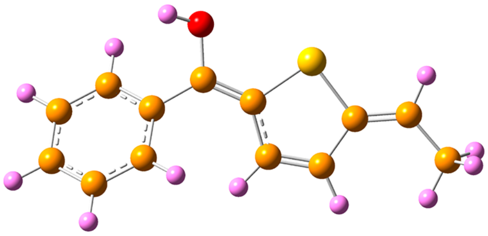

Figure 11. The optimized geometry structure of TBP calculated at the (U)B3LYP/6-311G(d,p) level of theory.

The TBP^3 intermediate has an absorption band at about 369 nm and was generated from the TB^3 intermediate by a protonation reaction. Then, the TBP^3 intermediate decays to TBP by an ISC process and TBP has its main absorption band at about 450 nm. Consequently, the growth time constant of 152 ± 5 ns (see Figure 13a$_1$) obtained from a monoexponential function fitting at 360 nm within 600 ns can be attributed to the formation time of the TBP^3 species; the decay time constants of 17 ± 0.3 nd 418 ± 6 μs (see Figure 13b$_1$) derived from a biexponential function fitting at 360 nm from 2 μs to about 2.5 ms are assigned to the lifetimes of TBP^3 and TBP intermediates; the decay time constant of 457 ± 8 μs (see Figure 13c$_1$) determined from a monoexponential function fitting at 450 nm from 280 μs to about 2.5 ms is attributed to the decay of the TBP species.

Investigation of the Transient Species and the Final Product by ns-TR^3 Spectroscopy. Photoinduced decarboxylation has been found to be an efficient and general reaction for different types of arylcarboxylic acids in aqueous solutions at pH > pK_a.[12] In a prior section, a proposed photodecarboxylation mechanism that occurs in a neutral PBS aqueous solution was given on the basis of the results of the fs-TA and ns-TA experimental spectra. The transient absorption spectra observed are relatively broad and featureless and similar to one another, since many of the transient species have a similar chromophore. ns-TR^3 spectra can help provide new insight into the identity, structure, and properties of several transient species associated with the photo-decarboxylation reaction observed in the degradation process of TPA. Figure 14 displays ns-TR^3 spectra obtained using a 266 nm pump wavelength and a 341 nm probe wavelength for an ~1 mM TPA neutral PBS aqueous solution.

Inspection of Figure 14 shows that four species are generated from 0 ns to 500 μs. In the early time spectra, only two main Raman bands located at 1593 and 1325 cm^{-1} were observed. As the delay time increases, the Raman band at 1325 cm^{-1} gradually decreases and then disappears, while the band at 1593 cm^{-1} increases in intensity and a new Raman band appears at 1542 cm^{-1} band and increases in intensity within about 1 μs. Subsequently, both Raman bands at 1542 and 1593 cm^{-1} begin to decrease in intensity accompanied by the appearance of another new Raman band at 1635 cm^{-1}

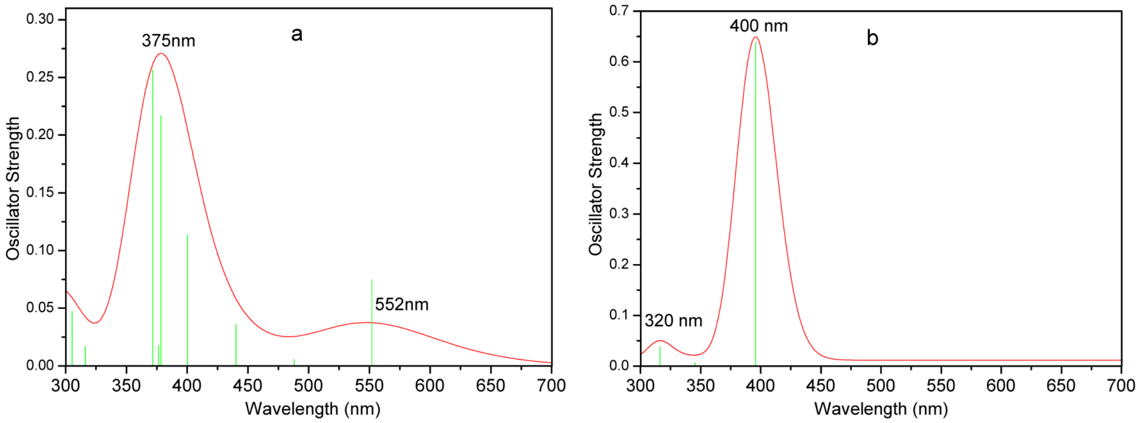

Figure 12. The predicted absorption spectra of the TBP^3 (a) and TBP (b) species obtained from the TD-DFT calculations done at the (U)B3LYP/6-311G(d,p) level of theory (see text for details).

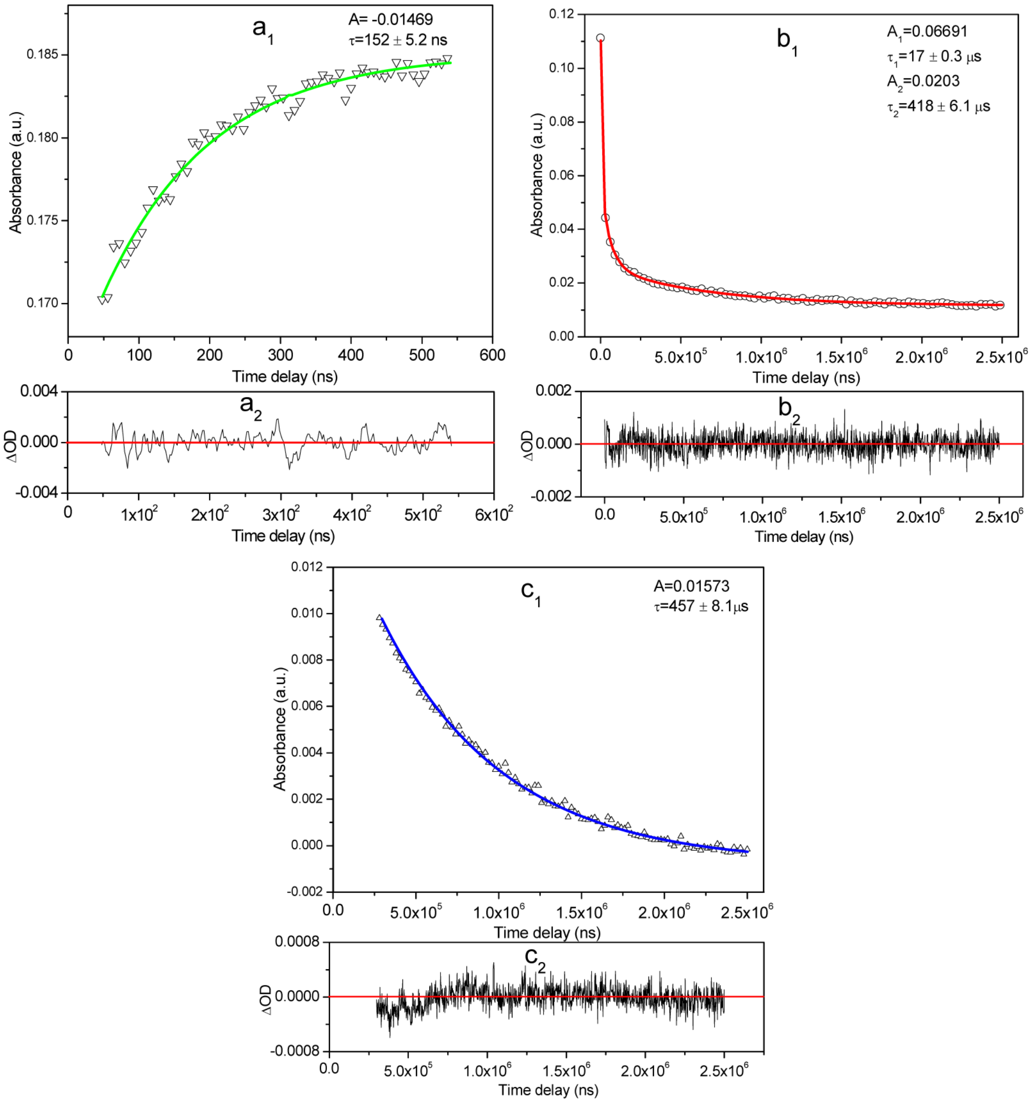

Figure 13. The kinetics of absorption bands of TPA obtained in neutral PBS solution at 363 nm early stage, a_1, fitting residual distribution, a_2, at 363 nm late stage, b_1, fitting residual distribution, b_2, and at 450 nm, c_1, fitting residual distribution, c_2. Note: A is the fitting parameter.

generated and increase in intensity before 100 μs. At the longest time delays examined, both Raman bands at 1542 and 1635 cm^{-1} decreased in intensity, while no obvious decrease in intensity was observed for the band at 1593 cm^{-1}. In addition, a strong Raman band was observed at 1442 cm^{-1} that increased in intensity from about 100 to 500 μs and this appears to correspond to the decrease in intensity of the Raman bands at 1542 and 1635 cm^{-1} over the same time region. The changes observed in the ns-TR^3 spectra indicate that there are four species present from 5 ns to 500 μs and the earlier species appear to be the precursors for the later time species. The analysis of the fs-TA and ns-TA results indicated an excited triplet was involved in the photo-decarboxylation reaction, and it is interesting to note this is different from the photo-decarboxylation of *o*-acetylphenyl-acid that was found to start from a highly excited singlet state with charge-transfer character.[48] This could possibly be due to the acid chain of *o*-acetylphenyl-acid being much closer to the carboxyl group so as to better facilitate an intramolecular proton transfer to the carboxyl group in the (π, π^*) state.

To help identify what transient species can be produced from the photo-decarboxylation reaction of TPA, calculations were done to find the optimized geometry and vibrational frequencies for likely species. The comparisons between some of the experimental ns-TR^3 spectra and the predicted Raman spectra for some possible transient species like TB^3 and TBP^3 are shown in Figure 15. The Raman bands at 1541 and 1594 cm^{-1} are characteristic bands for the TBP^3 species based on the good agreement between the spectra shown in Figure 15a for the predicted Raman spectrum of TBP^3 and the 400 ns TR^3 spectrum shown in Figure 15b. In addition, inspection of Figure 15b and c shows that the Raman bands at 1541 and 1594 cm^{-1} increase in intensity relative to the lower frequency Raman bands in the 1100−1500 cm^{-1} region and also new Raman bands appear in this spectral region with an increase in delay time from 10 to 400 ns. This indicates that more than one species coexist in the 10 and 400 ns spectra, and their relative populations change substantially between 10 and 400 ns. The 400 ns TR^3 spectrum appears to be mostly due to the TBP^3 intermediate. The 10 ns TR^3 Raman bands in the 1100−1500 cm^{-1} region shown in Figure 15c exhibit good agreement with the vibrational frequency pattern for the predicted Raman spectrum of the TB^3 species shown in Figure 15d. This and the noticeable presence of the 1541 and 1594 cm^{-1} Raman bands

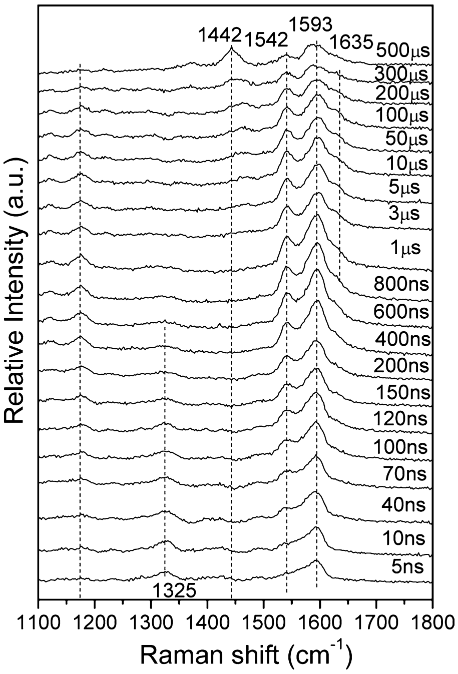

Figure 14. The ns-TR^3 spectra of 1 mM TPA in a neutral PBS aqueous solution obtained using a 266 nm wavelength pump and a 341 nm wavelength probe.

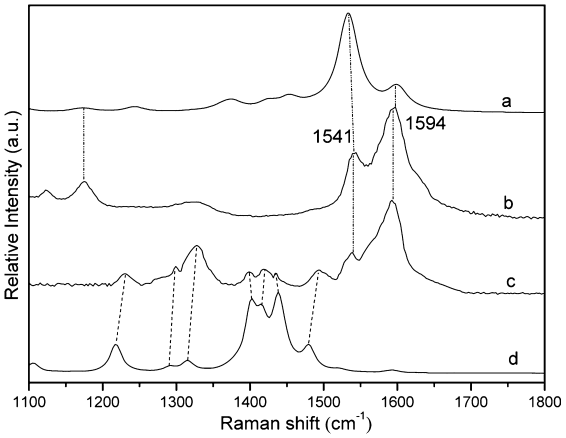

Figure 15. Comparison of the DFT predicted spectrum for the TBP^3 intermediate (a) and the TB^3 intermediate (d) with the experimental ns-TR^3 spectra of TPA in a neutral PBS aqueous solution acquired at a time delay of 10 ns (c) and 400 ns (b).

that are characteristic bands for the TBP^3 species indicate that both the TB^3 and TBP^3 intermediates noticeably contribute to the experimental 10 ns TR^3 spectrum. The ns-TA spectra along with the predicted absorption spectra also indicated that the TB^3 undergoes a protonation process to produce the TBP^3 intermediate on a similar time scale. The TR^3 spectral results here are consistent with the ns-TA results. The ns-TR^3 results also provide (to our knowledge) the first time-resolved vibrational spectroscopic characterization of these two key intermediates and confirm that the protonation reaction takes place on the nanosecond time scale in TPA after the decarboxylation on the picosecond time scale produces the TB^3 biradical intermediate. In summary, during the early nanosecond delay times, the TB^3 and TBP^3 intermediates coexist and the former one was the predominant species at 10 ns in Figure 15c and then the TB^3 gradually undergoes protonation to form TBP^3 which becomes the predominant species at 400 ns in the TR3 spectra shown in Figure 15b.

The calculated optimized structure of TBP^3 is shown in Figure 5S (Supporting Information), and the distribution of the spin density is displayed in Figure 16. Inspection of Figure 16 shows that the spin density is mainly located on the C_{12} and C_{21} atoms. Thus, it can be concluded that the TBP^3 species has a biradical character. A similar result has been suggested by Eriksson and co-workers[24] that a prompt photo-decarboxylation of the triplet conjugate base of TPA takes place to produce a carbanion, and its biradical form is the more stable resonance structure. Our TR^3 results experimentally confirm that this is the case.

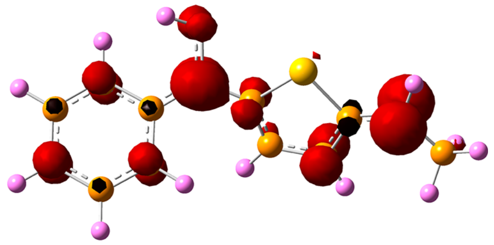

Figure 16. The Mulliken spin distribution for the TBP^3 species calculated at the UB3LYP/6-311G(d,p) level of theory.

Most of the Raman bands observed for the TBP^3 species are due to vibrations associated with the C−C stretch motions of the phenyl rings. For example, the Raman bands located at 849, 1329, 1355, and 1575 cm^{-1} are mainly due to these kinds of vibrational modes. The Raman band at 1171 cm^{-1} has contributions not only from the C−C stretch motions but also from a C−H bend motion. The calculated optimized structure in Figure 5S (Supporting Information) for the TBP^3 intermediate reveals a delocalization of the radical electrons into the aromatic ring, making the C−C bond length change to become about 1.4 Å, which stabilizes the triplet state. More detailed information for the vibrational modes associated with the observed Raman frequencies is presented in Table 8S (Supporting Information) and compared to the corresponding calculated vibrational frequencies for the TB^3 and TBP^3 intermediates.

On the basis of the conclusions of ns-TA spectra that TBP^3 will decay to its singlet form TBP, the predicted normal Raman spectrum of TBP was compared with the experimental spectrum obtained at a 120 *μ*s delay time and the comparison of these spectra is displayed in Figure 17. Examination of Figure 17 reveals the good agreement between the vibrational frequency patterns in the two spectra. The differences in the relative intensities between the experimental and calculated spectra are attributed to the TR^3 spectrum being resonantly enhanced, whereas the DFT calculations are for the normal Raman spectrum that is not resonantly enhanced. More detailed information for the comparison and assignment of experimental and calculated Raman bands are given in Table 9S of the Supporting Information.

Most of the Raman bands observed for the TBP species are due to the vibrations associated with the C−C stretch motions of the phenyl rings. For example, the Raman bands at 1329, 1609, and 1635 cm^{-1} are mainly due to these kinds of vibrational modes. The Raman band at 1635 cm^{-1} has contributions not only from the C−C stretch modes but also

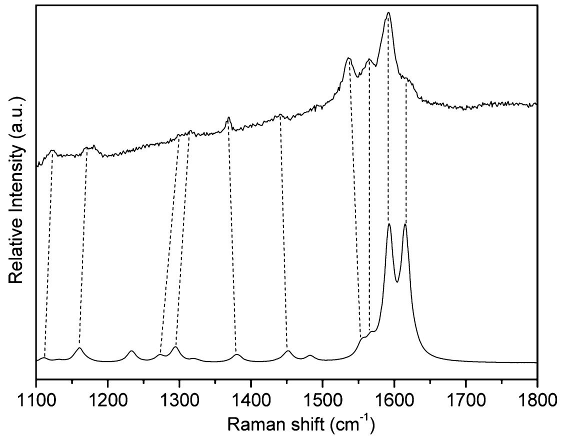

Figure 17. Comparison of the experimental ns-TR^3 spectrum of TPA in a neutral PBS aqueous solution acquired at a time delay of 120 μs (top) with the DFT predicted spectrum for the TBP intermediate (bottom).

from an O−H bend motion. The results for the ns-TA and the TR^3 spectra both indicate that, within a 100 μs delay time, the TB^3 intermediate undergoes a fast protonation process to generate the TBP^3 intermediate that also has some biradical character like the TB^3 intermediate. The TBP^3 intermediate subsequently undergoes ISC to form the singlet TBP intermediate.

In view of the instability of TBP that has appreciable enol character, one could expect further reaction may take place to produce the DTPA final product. Further inspection of Figure 14 shows that an obvious new Raman band is generated at 1442 cm^{-1} and this can be attributed to a final product DTPA characteristic Raman band. Figure 18 presents a comparison between the experimental ns-TR^3 spectrum at a 500 μs delay time and a DFT calculated Raman spectrum for the DTPA final product. The vibrational frequency patterns between the experimental 500 μs ns-TR^3 spectrum and the DFT calculated spectrum for the DTPA in Figure 18 are in good agreement with one another and indicate the 500 μs ns-TR^3 spectrum is mainly due to the DTPA final product. More detailed information for the experimental and computational Raman DTPA spectral results is given in Table 10S of the Supporting Information.

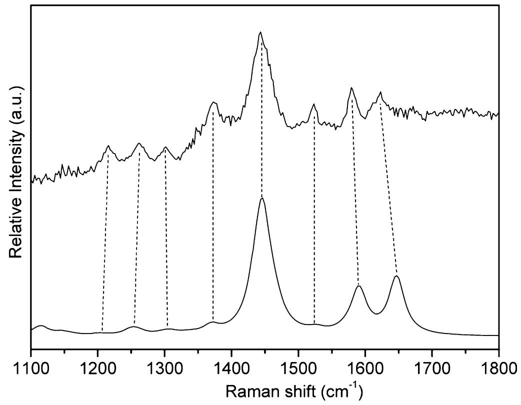

Figure 18. Shown is a comparison of the experimental ns-TR^3 spectrum of TPA in neutral PBS solution acquired at a time delay of 500 μs (top) with the DFT calculated normal Raman spectrum for the DTPA final product (bottom).

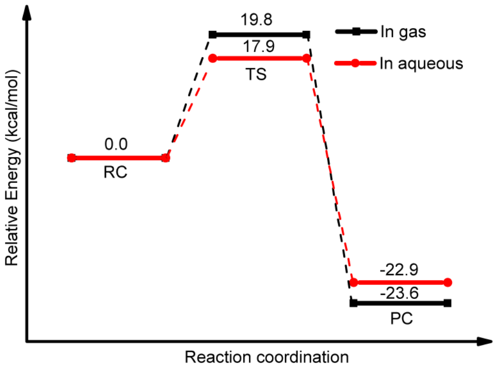

Figure 19. The reactive energy profile obtained from the DFT calculations for isomerization in gas and aqueous phases.

DFT calculations were done to estimate the activation energy for the reaction of TBP to form the DTPA final product in the gas phase and in aqueous solution. These DFT calculations found that the reaction barriers were 19.8 kcal/mol in the gas phase and 17.9 kcal/mol (see Figure 19) with consideration of a solvation effect by means of the PCM using UFF radii in aqueous solution (see the Supporting Information for details of the calculations). The optimized geometries of the reactant complex (RC), transient state (TS), and product complex (PC) of the reaction pathway are shown in Figure 6S (Supporting Information), and the structures are labeled by selected bond length values (in Å). The reaction barriers are reasonably consistent with the kinetics time constant in the 400−500 μs range for the formation of the DTPA final product in the ns-TA and ns-TR^3 spectra. We also performed DFT calculations to estimate the absorption spectrum of DTPA using the TD-B3LYP/6-311G(d,p) level of theory and consideration of the solvation effect by means of PCM using UAHF radii (see Figure 7S and Table 6S, Supporting Information, for the calculation results), and we found that DTPA has a larger oscillator strength estimated absorption band at 341 nm which is consistent with the ns-TA and ns-TR^3 spectra results.

Scheme 3 presents a reaction mechanism for the photochemistry of TPA$^-$ in a near neutral PBS aqueous solution based on our present time-resolved spectroscopy experiments that directly observed and characterized key reaction intermediates from femtoseconds to the formation of the DTPA final product. Scheme 4 presents a similar reaction mechanism based on time-resolved spectroscopic observations for the photochemistry of KP$^-$ in a near neutral PBS aqueous solution. Comparison of Schemes 3 and 4 shows that, while the sequence of events for the TPA$^-$ and KP$^-$ drugs in a near neutral PBS aqueous solution are similar to one another, there are some significant differences when the phenyl ring connecting the carbonyl group to the carboxyl containing side chain in KP$^-$ is replaced by a thiophene ring in TPA$^-$. For example, the ISC time becomes faster from S$_1$ to T$_1$ to have a rate constant of 3.0 ps for TPA$^-$ compared to a rate constant of about 8.8 ps for KP$^-$. This can be partially attributed to a heavy atom effect due to the presence of sulfur (S) in the thiophene ring of TPA$^-$. An intriguing effect is that the decarboxylation time constant is also faster in TPA$^-$ (about 320 ps) compared to KP$^-$ (about 568 ps), and this may be related to the thiophene stabilization of the TB^3 biradical intermediate (lifetime of about 152 ns) produced from the decarboxylation of the triplet TPA$^-$ compared to the ^{3}BC$^-$ biradical

Scheme 3. Proposed Reaction Mechanism for the Ultraviolet Excitation of TPA in a Near Neutral PBS Aqueous Solution Based on the Direct Time-Resolved Spectroscopy Observations of This Study from Femtoseconds to the Formation of the DTPA Final Product

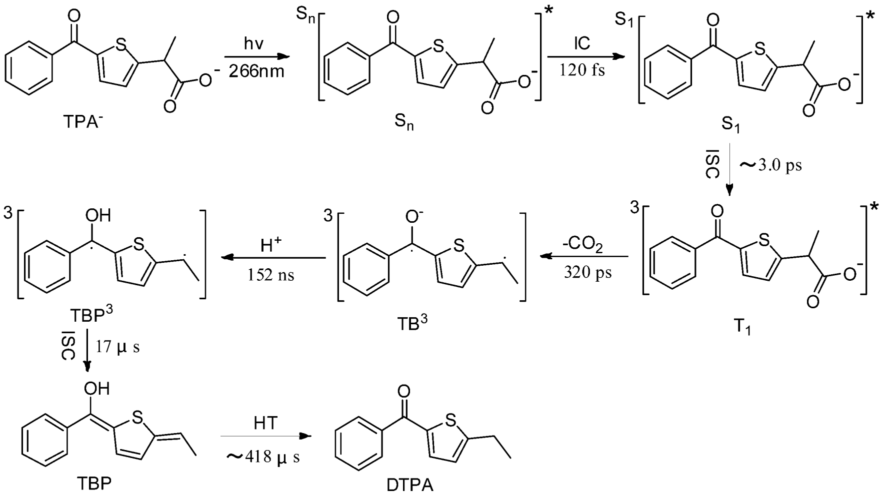

Scheme 4. Proposed Reaction Mechanism of KP after Ultraviolet Photo-Excitation in a Near Neutral PBS Aqueous Solution Based on the Direct Time-Resolved Spectroscopy Observations in the Literature[27,31]

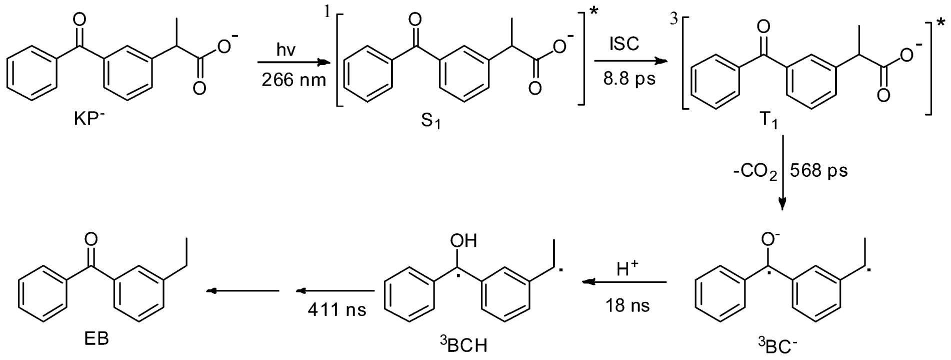

intermediate (lifetime of about 18 ns) formed from the decarboxylation of the triplet KP$^-$. This stabilization of the thiophene containing biradical anion intermediate from the decarboxylation reaction appears linked to a slower protonation of this biradical which results in a longer lifetime. The protonated biradical species containing a thiophene moiety (TBP^3) also has a very long lifetime of about 17 μs compared to the lifetime of about 411 ns for the analogous protonated biradical (^{3}BCH) associated with the photochemistry of KP$^-$ that has a phenyl ring instead of thiophene. The thiophene moiety leads to substantially longer lifetimes for both the anion biradical and its protonated biradical species. It will be interesting in the future to study the chemical reactivity of these biradical species that contain a thiophene versus a phenyl ring connecting the carbonyl group to the carboxyl containing side chain in aromatic carbonyl NSAIDs. In so far as the biradical intermediates are linked to phototoxicity of these NSAIDs, their properties and chemical reactivity to biological components should provide additional insights into the phototoxicity of these kinds of drugs.

■ CONCLUSION

The photo-decarboxylation and overall reaction mechanism for the photochemistry of TPA in a near neutral PBS aqueous solution was explored using fs-TA, ns-TA, and ns-TR^3 spectroscopy methods and also using DFT calculations. In the fs-TA spectra, a strong transient absorption band at 358 nm associated with the TPA$^-$ $S_n \rightarrow S_1$ was observed and then the S_1 intermediate underwent a fast ISC process to mainly transform to the T_1 state, which is characterized by two transient absorption bands at 360 and 600 nm. Subsequently, T_1 underwent decarboxylation to generate a triplet biradical species TB^3, which was clearly detected in the fs-TA and ns-TA spectra. Due to the higher pK_a value of TB^3 than the pH value of the near neutral PBS aqueous solution, protonation appeared to take place easily to produce the neutral species TBP^3. In both the ns-TA and ns-TR^3 spectra, the growth of TBP^3 was directly observed and then the TBP^3 intermediate decayed mostly by ISC to produce its singlet form TBP. The ns-TA and ns-TR^3 spectra also directly observed the reaction of the TBP intermediate to form the final product DTPA. The time-resolved spectroscopy experiments presented here have observed all of the intermediate species from femtoseconds to production of the major final product DTPA for the photochemistry of TPA$^-$ in a near neutral PBS aqueous solution. The ns-TR^3 experiments also have provided the first time-resolved vibrational spectroscopic characterization of several key intermediates to clearly identify them and gain more insight into their structure and properties. Comparison of the time-resolved spectroscopy results here for TPA$^-$ to those reported in the literature for the related KP$^-$ compound under similar conditions indicate that the thiophene moiety in TPA$^-$ that replaces one phenyl ring in KP$^-$ leads to a faster ISC from S$_1$ to T$_1$ and also a faster decarboxylation of the T$_1$ intermediate to produce the anionic biradical intermediate (TB^3 in Scheme 3 compared to ^{3}BC$^-$ in Scheme 4). In addition, the lifetimes of the anionic biradical intermediate and its protonated biradical intermediate is much longer for the TPA$^-$ associated species (TB^3 and TBP^3 in Scheme 3) than the KP$^-$ ones (^{3}BC$^-$ and ^{3}BCH in Scheme 4).

■ ASSOCIATED CONTENT

Ⓢ Supporting Information

The TD-DFT predicted absorption spectrum of the TPA$^-$ species is given. The fs-TA spectra of TPA in MeCN solvent are provided. The DFT calculated frontier orbitals of TPA$^-$ involved in the HOMO-3, LUMO, and LUMO+2 orbitals are given. The chemical structure of TB^3 is given. The fs-TA spectra and their kinetics monitored at 352 nm of TPA in a pure MeCN solvent are shown. The DFT optimized structure of TBP^3 is given. The optimized geometries of the RC, TS, and PC obtained from the DFT calculations for the reaction of TPA are given. The DFT predicted absorption spectrum of the DTPA final product is given. The DFT Mulliken charge distribution and spin distribution of the TB^3 species are given. Excited-state energies and oscillator strengths determined from DFT calculations are shown for the ground state TPA$^-$, the TB^3 intermediate, the TBP^3 intermediate, the TBP species, and the final product are given. Comparisons of the experimental resonance Raman or ns-TR^3 spectra vibrational frequencies with the DFT calculated vibrational frequencies for the TPA$^-$ species, the TB^3 and TBP^3 intermediates, the TBP species, and the DTPA final product with preliminary vibrational assignments and qualitative descriptions of the vibrational modes in the 800−1800 cm^{-1} region are presented. The Cartesian coordinates used in the calculations of all the intermediates are provided. The full ref 39 is given. This material is available free of charge via the Internet at http://pubs.acs.org.

■ AUTHOR INFORMATION

Corresponding Author

*Fax: (+852) 2597-1586. Phone: (+852) 2859 2160. E-mail: phillips@hku.hk.

Notes

The authors declare no competing financial interest.

■ ACKNOWLEDGMENTS

This work was supported by a grant from the Research Grants Council of Hong Kong (HKU 7035/08P) and the University Grants Committee Special Equipment Grant (SEG-HKU-07) to D.L.P. Support from the University Grants Committee Areas of Excellence Scheme (AoE/P-03/08) is also gratefully acknowledged.

■ REFERENCES

(1) Ljunggren, B. *Photodermatology* **1985**, *2*, 3−9.

(2) Przybilla, B.; Schwab-Przybilla, U.; Ruzicka, T.; Ring, J. *Photodermatology* **1987**, *4*, 73.

(3) Castell, J. V.; Gomezlechon, M. J.; Grassa, C.; Martinez, L. A.; Miranda, M. A.; Tarrega, P. *Photochem. Photobiol.* **1994**, *59*, 35−39.

(4) Miranda, M. A.; Castell, J. V.; Gomezlechon, M. J.; Hernandez, D.; Martinez, L. A. *Toxicol. In Vitro* **1995**, *9*, 499−503.

(5) Castelli, F.; De Guidi, G.; Giuffrida, S.; Miano, P.; Sortino, S. *Int. J. Pharm.* **1999**, *184*, 21−33.

(6) Agapakis-Causse, C.; Bosca, F.; Castell, J. V.; Hernandez, D.; Marin, M. L.; Marrot, L.; Miranda, M. A. *Photochem. Photobiol.* **2000**, *71*, 499−505.

(7) Bosca, F.; Miranda, M. A.; Morera, I. M.; Samadi, A. *J. Photochem. Photobiol., B* **2000**, *58*, 1−5.

(8) Miranda, M. A.; Lahoz, A.; Bosca, F.; Metni, M. R.; Abdelouahab, F. B.; Castell, J. V.; Perez-Prieto, J. *Chem. Commun.* **2000**, *22*, 2257−2258.

(9) Romani, A.; Ortica, F.; Favaro, G. *J. Photochem. Photobiol., A* **2000**, *135*, 127−134.

(10) Sortino, S.; Cosa, G.; Scaiano, J. C. *New J. Chem.* **2000**, *24*, 159−163.

(11) Starrs, S. M.; Davies, R. J. H. *Photochem. Photobiol. Sci.* **2000**, *72*, 291−297.

(12) Xu, M. S.; Wan, P. *Chem. Commun.* **2000**, *21*, 2147−2148.

(13) Bosca, F.; Marin, M. L.; Miranda, M. A. *Photochem. Photobiol. Sci.* **2001**, *74*, 637−655.

(14) Miranda, M. A. *Pure Appl. Chem.* **2001**, *73*, 481−486.

(15) Monti, S.; Encinas, S.; Lahoz, A.; Marconi, G.; Sortino, S.; Perez-Prieto, J.; Miranda, M. A. *Helv. Chim. Acta* **2001**, *84*, 2452−2466.

(16) Samadi, A.; Martinez, L. A.; Miranda, M. A.; Morera, I. M. *Photochem. Photobiol. Sci.* **2001**, *73*, 359−365.

(17) Sortino, S.; Martinez, L. J.; Marconi, G. *New J. Chem.* **2001**, *25*, 975−980.

(18) delaPena, D.; Marti, C.; Nonell, S.; Martinez, L. A.; Miranda, M. A. *Photochem. Photobiol. Sci.* **1997**, *65*, 828−832.

(19) Martinez, L. J.; Scaiano, J. C. *J. Am. Chem. Soc.* **1997**, *119*, 11066−11070.

(20) Encinas, S.; Miranda, M. A.; Marconi, G.; Monti, S. *Photochem. Photobiol. Sci.* **1998**, *67*, 420−425.

(21) Bosca, F.; Miranda, M. A. *Photochem. Photobiol. Sci.* **1999**, *70*, 853−857.

(22) Encinas, S.; Miranda, M. A.; Marconi, G.; Monti, S. *Photochem. Photobiol. Sci.* **1998**, *68*, 633−639.

(23) Vinette, A. L.; McNamee, J. P.; Bellier, P. V.; McLean, J. R. N.; Scaiano, J. C. *Photochem. Photobiol. Sci.* **2003**, *77*, 390−396.

(24) Musa, K. A. K.; Eriksson, L. A. *J. Phys. Chem. B* **2009**, *113*, 11306−11313.

(25) Ma, J. N.; Cheng, S. C.; An, H. Y.; Li, M. D.; Ma, C. S.; Rea, A. C.; Zhu, Y.; Nganga, J. L.; Dore, T. M.; Phillips, D. L. *J. Phys. Chem. A* **2011**, *115*, 11632−11640.

(26) Ma, J. N.; Li, M. D.; Phillips, D. L.; Wan, P. *J. Org. Chem.* **2011**, *76*, 3710−3719.

(27) Li, M. D.; Ma, J. N.; Su, T.; Liu, M. Y.; Yu, L. H.; Phillips, D. L. *J. Phys. Chem. B* **2012**, *116*, 5882−5887.

(28) Ma, J. N.; Rea, A. C.; An, H. Y.; Ma, C. S.; Guan, X. G.; Li, M. D.; Su, T.; Yeung, C. S.; Harris, K. T.; Zhu, Y.; Nganga, J. L.; Fedoryak, O. D.; Dore, T. M.; Phillips, D. L. *Chem.—Eur. J.* **2012**, *18*, 6854−6865.

(29) Ma, C. S.; Kwok, W. M.; Chan, W. S.; Du, Y.; Zuo, P.; Kan, J. T. W.; Toy, P. H.; Phillips, D. L. *Curr. Sci.* **2009**, *97*, 202−209.

(30) Li, M. D.; Du, Y.; Chuang, Y. P.; Xue, J. D.; Phillips, D. L. *Phys. Chem. Chem. Phys.* **2010**, *12*, 4800−4808.

(31) Li, M. D.; Yeung, C. S.; Guan, X.; Ma, J.; Li, W.; Ma, C. S.; Phillips, D. L. *Chem.—Eur. J.* **2011**, *17*, 10935−10950.

(32) Ma, C. S.; Kwok, W. M.; An, H. Y.; Guan, X. G.; Fu, M. Y.; Toy, P. H.; Phillips, D. L. *Chem.—Eur. J.* **2010**, *16*, 5102−5118.

(33) Srinivasan, A.; Kebede, N.; Saavedra, J. E.; Nikolaitchik, A. V.; Brady, D. A.; Yourd, E.; Davies, K. M.; Keefer, L. K.; Toscano, J. P. *J. Am. Chem. Soc.* **2001**, *123*, 5465−5472.

(34) Chan, P. Y.; Ong, S. Y.; Zhu, P. Z.; Zhao, C. Y.; Phillips, D. L. *J. Phys. Chem. A* **2003**, *107*, 8067−8074.

(35) Cances, E.; Mennucci, B.; Tomasi, J. *J. Chem. Phys.* **1997**, *107*, 3032−3041.

(36) Mennucci, B.; Tomasi, J. *J. Chem. Phys.* **1997**, *106*, 5151−5158.

(37) Cossi, M.; Barone, V.; Mennucci, B.; Tomasi, J. *Chem. Phys. Lett.* **1998**, *286*, 253−260.

(38) Tomasi, J.; Mennucci, B.; Cammi, R. *Chem. Rev.* **2005**, *105*, 2999−3093.

(39) Frisch, M. J.; Trucks, G. W.; Schlegel, H. B.; Scuseria, G. E.; Robb, M. A.; Cheeseman, J. R.; Montgomery, J. A., Jr.; Vreven, T.; Kudin, K. N.; Burant, J. C.; et al. *Gaussian 03*; Gaussian, Inc.: Wallingford, CT, 2004.

(40) Fillet, M.; Bechet, I.; Piette, V.; Crommen, J. *Electrophoresis* **1999**, *20*, 1907−1915.

(41) *Modern Molecular Photochemistry*; Turro, N. J., Ed.; University Science Books: Sausalito, CA, 1991.

(42) Chuang, Y. P.; Xue, J. D.; Du, Y.; Li, M. D.; An, H. Y.; Phillips, D. L. *J. Phys. Chem. B* **2009**, *113*, 10530−10539.

(43) Musa, K. A. K.; Matxain, J. M.; Eriksson, L. A. *J. Med. Chem.* **2007**, *50*, 1735−1743.

(44) O'Boyle, N. M.; Tenderholt, A. L.; Langner, K. M. *J. Comput. Chem.* **2008**, *29*, 839−845.

(45) Suzuki, H.; Suzuki, T.; Ichimura, T.; Ikesue, K.; Sakai, M. *J. Phys. Chem. B* **2007**, *111*, 3062−3068.

(46) Suzuki, T.; Okita, T.; Osanai, Y.; Ichimura, T. *J. Phys. Chem. B* **2008**, *112*, 15212−15216.

(47) Suzuki, T.; Osanai, Y.; Isozaki, T. *Photochem. Photobiol.* **2012**, *88*, 884−888.

(48) Ding, L.; Chen, X. B.; Fang, W. H. *Org. Lett.* **2009**, *11*, 1495−1498.